Cell type-dependent control of p53 transcription and enhancer activity by p63

Gizem Karsli Uzunbas, Faraz Ahmed, and Morgan A. Sammons*

Department of Biological Sciences, State University of New York at Albany, Albany, NY 12222

* Corresponding Author: masammons@albany.edu

Abstract

Transcriptional activation by p53 provides powerful, organism-wide tumor suppression. In this work, we demonstrate that the p53-induced transcriptome is dependent on pre-establishment of cell type-dependent *cis*-regulatory networks. The epithelial-specific p53 transcriptome is strongly dependent on the p53 family member p63, which acts as a pioneer factor for epithelial-specific enhancers. These results suggest a broad mechanism for regulating the p53-dependent cellular response to stress through differential regulation of *cis*-regulatory elements and identify p63 as a direct and critical regulator of enhancer activity in epithelial cell types.

Introduction

The p53 family of transcription factors regulate highly diverse cellular functions, including tumor suppression and control of cell specification and identity (Levrero et al. 2000). p53 is a master tumor suppressor that protects organismal fidelity after exposure to cellular stress like DNA damage. This activity is dependent on p53's ability to activate transcription of a canonical network of genes involved in DNA damage repair, cell cycle arrest, apoptosis, and senescence (Kastenhuber and Lowe 2017). Surprisingly, many of these transcriptional pathways are individually dispensable for tumor suppression, suggesting p53 regulates a redundant and not-yet fully characterized transcriptional network (Andrysik et al. 2017; Li et al. 2012).

Genetic inactivation of the p53 tumor suppressor pathway is highly recurrent across cancer types. p53 mutations, while frequent, vary depending on the tumor type with additional genetic and epigenetic mechanisms proposed to inactivate the p53 pathway in the presence of wild-type p53 (Zhu et al. 2016; Ciriello et al. 2013; Kandoth et al. 2013). p63 and p73, p53 family members, function similarly to p53 in the stress response, although their precise roles in tumor suppression are unresolved (Flores et al.

36 2002; Botchkarev and Flores 2014; DeYoung and Ellisen 2007). p63 and p73 are
37 primarily lineage restricted to epithelial cell types where each serves critical and non-
38 overlapping roles in cell identity and self-renewal (Melino et al. 2015; Levrero et al.
39 2000). Mutations within p63 are causative for a number of epithelial-associated human
40 developmental disorders independent of p53 activity, and mutations in p63 target genes
41 underlie similar phenotypes (Fakhouri et al. 2014; Brunner et al. 2002). A significant and
42 still outstanding question involves dissection of specific roles and functional interplay
43 between p53 family members during development, in the regulation of cellular
44 homeostasis, and in the etiology of disease.
45 The similarity between DNA binding motifs suggested that competition for binding
46 sites serves a central role in the regulation of p53 family member activity (Moll et al.
47 2001; Billant et al. 2016). Indeed, previous studies implicate the ΔNp63 isoforms,
48 lacking transactivation domains, as direct repressors of the p53-induced transcriptome
49 through a binding site competitive mechanism (Yang et al. 2006, 1998; Mundt et al.
50 2010). Amplification of p63 is thought to drive a number of epithelial cancers,
51 particularly squamous cell carcinomas, although both p53-dependent and independent
52 mechanisms have been proposed for this driver activity (Saladi et al. 2017). As the
53 majority of cancers are derived from epithelial tissues, the mechanisms of p53 family
54 dependent tumor suppression in those tissues is of special interest (Kandoth et al.
55 2013).
56 Fate choice after p53 activation, be it apoptosis, temporary/permanent cell cycle
57 arrest, or continued proliferation, is variable across cell types suggesting that p53-
58 dependent transcription is also cell type-dependent (Kastenhuber and Lowe 2017). A
59 bevy of sensitive methodological approaches have been used to identify p53 binding
60 sites and gene targets across transformed and primary cell lines in an effort to explain
61 these terminal cell fate choices and p53-dependent tumor suppression. A recent set of
62 meta-analyses have suggested that p53 binding to the genome is invariant (Verfaillie et
63 al. 2016), proposing that p53 acts independently to drive gene expression of a core
64 tumor suppressor network across all cell types due to the low enrichment of other
65 transcription factor motifs at p53-bound enhancers and the reported pioneer factor
66 activity of p53 (Verfaillie et al. 2016; Andrysik et al. 2017; Younger and Rinn 2017).

67 Conversely, similar experimental approaches demonstrate cell type-specific p53 binding
68 and gene targets although the mechanisms driving these differential activities are
69 unknown (Hafner et al. 2017). Additional experimental evidence and models are
70 required to unravel these mutually exclusive p53 regulatory mechanisms.
71 We previously proposed that the local chromatin environment, including variable
72 chromatin accessibility and enhancer activity, contributes to novel p53 activities across
73 cell types (Sammons et al. 2015). To address this question, we performed genomewide
74 transcriptome, epigenome, and p53 cistrome profiling in primary dermal foreskin
75 fibroblasts (SkFib) and breast epithelial (MCF10A) cell lines, two cell types with varying
76 enhancer activity at p53 binding sites (Sammons et al. 2015). Our results directly
77 implicate differential *cis*-regulatory element activity as a mediator of the p53 network,
78 with both promoter and enhancer activity contributing to p53-dependent gene
79 expression differences. Further, we have identified the p53 family member p63 as one
80 factor that drives the epithelial-specific p53 transcriptome through an enhancer
81 maintenance activity. We further propose that p63 serves as licensing factor for a set of
82 epithelial-specific enhancers. Thus, these data support a mechanism whereby co-
83 operating transcription factors control cell type-dependent *cis*-regulatory networks that
84 regulate p53 activity.
85
86 **Results and Discussion**
87 We used polyA-enriched RNA-seq to assess gene expression dynamics in model
88 cell lines (MCF10A and SkFib) after p53 activation in response to Nutlin-3A treatment
89 (Fig. 1A, Supplemental Fig. S1A). We reasoned Nutlin-3A, a non-genotoxic activator of
90 p53, would better reflect p53-dependent transcriptional activity relative to genotoxic
91 activation methods as DNA damage-dependent, but p53-independent, signaling would
92 not confound our analysis (Vassilev et al. 2004; Allen et al. 2014). Consistent with a cell
93 type-dependent activity of p53, MCF10A cells displayed a broad and specific set of
94 Nutlin-3A-induced genes, whereas SkFib showed a markedly smaller, albeit specific,
95 p53-activated transcriptome (Fig. 1B). Orthogonal validation by qRT-PCR confirmed a
96 stringent cell type-specificity of each set of genes and demonstrated that canonical p53
97 targets, like *CDKN1A* and *BTG2* are indeed shared across cell types (Supplemental Fig.
98 S1B-D). Decreasing the fold-change cutoff yielded an increased number of differentially

99 regulated genes for each cell type, but maintained the trend that p53-dependent gene
100 targets are more abundant in MCF10A (Supplemental Fig. S1E). Genes upregulated in
101 both cell lines are significantly associated with the core p53 response (Supplemental
102 Fig. S1F), as expected. MCF10A-specific upregulated genes are enriched in gene
103 ontology groups related to establishment of the skin barrier and p53-dependent
104 processes like programmed cell death and homeostasis. In contrast, SkFib-specific
105 targets are enriched in other cellular stress-related pathways including those associated
106 with the hypoxia response and catabolic processes (Supplemental Fig. S1F,
107 Supplemental Table S1). The majority of the MCF10A-specific targets represent novel
108 p53-dependent genes and over 20% of SkFib-specific targets have not been observed
109 previously (Supplemental Fig. S1G, Supplemental Tables S2-3 (Fischer 2017)). These
110 initial analyses reveal that the p53-activated transcriptome is highly variable between
111 non-transformed cell types and may reflect the need for tailored, cell specific responses
112 to p53 activation after cellular stress.
113 We next confirmed that a set of cell type-specific targets were p53-dependent
114 (Fig. 1C-D, Supplemental S1H). Indeed, knockdown of p53 in SkFib led to sharp
115 reduction in both basal and Nutlin-3A-induced expression of the SkFib-specific genes,
116 *GDNF* and *TRIM55* (Fig. 1D). Depletion of p53 in MCF10A (Fig. 1E, Supplemental Fig.
117 S1I) led to a loss of Nutlin-3A-induced *RIC3* and *IL1B* expression relative to a non-
118 targeting control shRNA (Fig. 1F), indicating these genes are *bona fide* p53 target
119 genes in epithelial cells.
120 Recent analyses reached opposing conclusions with regard to the cell type-
121 dependence of p53 engagement with the genome (Verfaillie et al. 2016; Hafner et al.
122 2017). We thus assessed whether differences in p53 engagement with the genome in
123 our model cell lines might explain our observations of cell type-dependent
124 transcriptomes. Consistent with cell type-dependence, genomewide ChIP-seq revealed
125 a highly-enriched set of MCF10A-specific p53 binding sites and a smaller number of
126 SkFib-specific sites, mirroring our gene expression observations (Fig. 1G). p53 binding
127 at common sites as measured by ChIP-seq mirrors both the basal and induced
128 expression of p53 (Supplemental Fig. S1J). p53 protein expression and binding do not
129 correlate with the ability to activate common targets as SkFib displayed dramatically

130 increased Nutlin-3A induced gene activation compared to MCF10A (Supplemental Fig.
131 S1K). Common p53 binding events are primarily within 10kb of genes upregulated in
132 both cell types, similar to previous results suggesting that many direct p53 targets have
133 proximal p53 binding (Supplemental Fig. S1L). MCF10A-specific genes have a higher
134 percentage of proximal p53 binding relative to SkFib. Notably, we observe both
135 MCF10A and SkFib p53 binding proximal to SkFib-specific genes. Cell type-specific
136 binding events displayed lower p53 occupancy than at common sites, suggesting that
137 common sites might represent more stable or higher affinity p53 binding sites
138 (Supplemental Fig. S1M). Taken together, these data provide evidence that the p53-
139 dependent transcriptome is indeed cell type-specific and that p53 engagement with the
140 genome is variable across cell types.

141 We next wanted to identify potential mechanisms driving the strong, cell type-
142 specificity within the p53 transcriptome and cistrome. The most straightforward
143 hypothesis is that differential p53 binding drives cell type-specific transcriptome
144 differences, but our data suggest that this might only explain MCF10A behavior (Fig.
145 1G, Supplemental Fig. S1L). Thus, we examined *GDNF*, a SkFib-specific gene, and
146 observed proximal p53 binding upstream of the *GDNF* transcriptional start site (Fig. 2A).
147 We also noted p53 binding to this region in MCF10A, even though p53-dependent
148 *GDNF* expression is SkFib-specific (Fig. 2A). Similar p53 proximal binding was
149 observed at SkFib-specific genes *TRIM55* and *MAMDC2* (Supplemental Fig. S2A),
150 suggesting that differential proximal p53 binding cannot explain the cell type-specificity
151 observed in SkFib relative to MCF10A. We and others previously proposed that
152 enhancer activity is critical for regulating p53-dependent gene expression(Sammons et
153 al. 2015; Sullivan et al. 2018). As enhancers also have a strong cell type-
154 dependence(Calo and Wysocka 2013; Heinz et al. 2015), we performed ChIP-seq
155 experiments for canonical promoter (H3K4me3) and enhancer-associated (H3K4me2,
156 H3K27ac) histone modifications to determine whether differentially active promoters or
157 enhancers might explain the observed cell type specificity of the p53 transcriptome.

158 The local chromatin environment at the *GDNF* proximal p53 binding site is
159 enriched for H3K27ac and H3K4me2, but lacks H3K4me3, suggestive of an active
160 enhancer in both cell types (dashed box, Fig. 2A). Consistent with high basal and p53-

161 inducible expression of *GDNF* in SkFib, the *GDNF* promoter is strongly enriched for the
162 canonical promoter-associated histone modification H3K4me3 (solid box, Fig. 2A) which
163 is completely absent from MCF10A. We observed differential promoter activity at other
164 SkFib-specific p53 target promoters (Supplemental Fig. S2A) without observed
165 differences in p53 binding. It is currently unclear whether the lack of activity in MCF10A
166 is driven by lack of promoter-bound cofactors, through repressive chromatin-associated
167 mechanisms, or both. Repressive DNA and histone methylation have been implicated in
168 differential control of p53 activity in cancer cell lines (Hermeking et al. 1997; Mungamuri
169 et al. 2012; París et al. 2008). These observations suggest that promoter competence,
170 independent of p53 binding, potently controls cell specific p53 transcription responses.
171 We then sought to better understand the mechanisms driving the epithelial-
172 specific p53 target genes. p53 binding is pervasive in MCF10A relative to SkFib (Fig.
173 1G), therefore we investigated the connection between *de novo* epithelial p53 binding
174 and the induction of specific targets. Examination of the MCF10A-specific targets *RIC3*
175 and *MYBPHL* revealed MCF10A-specific binding of p53 binding to putative intragenic
176 enhancers specifically in MCF10A (Fig. 2B, Supplemental Fig. S2B). This is consistent
177 with the lack of basal expression of *RIC3* mRNA in SkFib and p53-dependent activation
178 in MCF10A. We speculated that MCF10A-specific p53 binding might correlate with
179 enhancer signatures specific to epithelial cell types. MCF10A-specific p53 binding is
180 flanked by enrichment of MCF10A-specific H3K27ac and H3K4me2 (Fig. 2C). These
181 sites also lack H3K4me3 (Supplemental Fig. S2C), suggesting they are putative
182 enhancers. Common p53 binding sites are enriched for enhancer-associated chromatin
183 modifications in both cell types whereas cell type-specific p53 binding overlaps cell
184 type-specific enhancer modifications (Supplemental Fig. S2D-G). Taken together, these
185 data demonstrate that cell specific p53 binding is correlated with enhancers unique to
186 that cell type. These observations thus provide a putative mechanism for cell type-
187 dependent responses. Transcriptional activation requires both gene-proximal p53
188 binding and pre-establishment of *cis*-regulatory elements. While both are necessary,
189 neither is sufficient to confer p53-dependent gene activation.
190 We next investigated what might drive the cell type-dependence and activity of
191 p53-bound enhancers. Enhancer specification is generally believed to be regulated by

192 the combined effort of multiple common and lineage-dependent transcription factors
193 (Heinz et al. 2015). Multiple recent reports suggest that p53 activity at *cis*-regulator
194 elements is independent of any accessory transcription factors, primarily due to low
195 enrichment/specificity of other DNA motifs (Younger and Rinn 2017; Verfaillie et al.
196 2016; Sullivan et al. 2018). Indeed, MCF10A enhancers are highly enriched for
197 underlying p53/p63 motifs relative to SkFib, consistent with results from the FANTOM
198 consortium and a lack of any obvious epithelial-specific transcription factor motifs
199 (Supplemental Fig. S2H, Supplemental Table S4, (The FANTOM Consortium et al.
200 2014)). As the p53 family shares a common, although not identical, response element
201 motif, we speculated that p53 family members might regulate MCF10A-specific p53
202 binding events or enhancer activity and might explain previous observations.
203 Epithelial cells highly express p63 and are dependent on p63 activity for self-
204 renewal and epidermal commitment *in vivo* (Yang et al. 1999). p63 also bookmarks
205 enhancers during epidermal differentiation (Kouwenhoven et al. 2015) and may regulate
206 chromatin accessibility through interactions with chromatin modifiers (Bao et al. 2015;
207 Lin-Shiao et al. 2018). p63 is expressed only in MCF10A which do not express the other
208 p53 family member p73 (Supplemental Fig. S3A). Therefore, we focused on the function
209 of p63 in epithelial enhancer activity by performing genomewide ChIP-seq of p63 in
210 MCF10A after DMSO or Nutlin-3A treatment. Examination of *IL1B* and *RNASE7*,
211 MCF10A-specific p53 targets, displayed proximal p63 binding to distinct enhancer
212 regions co-occupied by p53 in an MCF10A-specific manner (Fig. 3A, Supplemental Fig.
213 S3B). Globally, p63 binds to significantly more genomic loci than does p53 (Fig. 3B), but
214 over 75% of epithelial-specific p53 binding events overlap p63 binding. Shared binding
215 sites display higher occupancy and are more likely to have enhancer-associated
216 chromatin modifications than do sites unique to either p53 or p63 (Fig. 3C,
217 Supplemental Fig. S3C), suggesting that both p53 and p63 might be necessary for full
218 enhancer activity.
219 Overall, p63 binding correlates with epithelial-specific enhancer modifications
220 and co-occupies the majority of p53 sites (Fig. 3B, Supplemental Fig. S3D). The modal
221 binding of p63 is within 10kB of the TSS of Nutlin-3A-induced genes, further suggesting
222 that p63 might co-regulate these specific target genes (Supplemental Fig. S3D). In

223 order to test whether p63 regulates p53 activity, we created MCF10A cells stably-
224 expressing shRNA against p63 (Fig. 3D, Supplemental Fig. S3E). We then performed
225 RNA-seq analysis of MCF10A cells expressing non-targeting (scr), p53, or p63 shRNA
226 to determine their relative contributions to epithelial-specific target genes. Loss of p53
227 expression strongly inhibited Nutlin-3A-induced gene expression consistent with this set
228 of genes representing true p53 targets (Fig. 3E). Knockdown of p63 showed more
229 pleiotropic effects. Globally, Nutlin-3A-induced target gene activation is inhibited in p63
230 knockdown relative to non-targeting controls, suggesting p63 activity is required for a
231 set of epithelial p53 targets (Fig. 3E). Whereas 40% of p53 target genes show defective
232 induction in the absence of p63, the remainder of the genes are either unaffected or
233 display increased p53-dependent transactivation (Supplemental Fig. S3F). This
234 observation is consistent with previous reports of direct repression of p53-dependent
235 transactivation through binding site competition (Mundt et al. 2010; Yang et al. 1998).
236 Our data suggest that p63 also functions to co-activate a set of p53-dependent
237 genes specifically in epithelial cell types. We then validated these results by qRT-PCR
238 on a panel of epithelial target genes after p53 or p63 knockdown. *RIC3,* previously
239 demonstrated to be a p53-dependent gene (Fig. 1F), is also derepressed and shows
240 higher p53-dependent transactivation in the absence of p63 (Fig. 3F). Conversely, both
241 *IL1A* and *IL1B* are dependent on p53 and p63 for full transactivation, with *IL1B* showing
242 a strong dependence on p63 for basal expression (Fig. 3F). Knockdown of p63 also led
243 to basal gene expression changes for p53 targets (Supplemental Fig. S3G) and genes
244 related to cell cycle and cell adhesion/extracellular matrix (Supplemental Table S5), as
245 has previously been described (Carroll et al. 2006).
246 In total, these results suggest that p63 functions as both a co-activator and
247 repressor of p53-dependent transcription in MCF10A, but the mechanisms driving these
248 activities were not clear. p53 and p63 engagement to the genome in epithelial cells
249 correlates with enhancer activity and the p53 family are putative pioneer factors with
250 enhancer bookmarking activity (Kouwenhoven et al. 2015; Bao et al. 2015; Sammons et
251 al. 2015; Cui and Zhurkin 2014). Therefore, we examined the effect of p53 and p63 on
252 enhancer identity in MCF10A. Globally, loss of p63 led to a dramatic reduction of
253 H3K27ac and H3K4me2 at p63-bound enhancers (Fig. 4A-B). Enhancer-associated

254 modifications were unaffected by loss of p53, nor were the genomewide complement of
255 enhancers affected by loss of either p53 or p63 (Fig. 4A-B), suggesting this is a
256 phenomenon specific to p63-bound enhancers. Expression of *RRM1*, a member of the
257 ribonucleotide reductase enzyme complex, was significantly downregulated by loss of
258 p63 and unaffected in the absence of p53. p63-bound enhancers upstream of *RRM1*
259 and *EDN2*, a p53 target gene, showed dramatic loss of H3K27ac and H3K4me2
260 enrichment in p63-depleted cells, with similar loss of enhancer-associated modifications
261 observed broadly at p63 binding sites (Fig. 4A-C, Supplemental Fig. S4A). In total, over
262 30% and 20% of p63-bound H3K27ac and H3K4me2 sites, respectively, showed at
263 least a 2-fold reduction in MCF10A-p63sh cells relative to scrambled shRNA (Fig. 4D).
264 The loss of enhancer-associated histone modifications at p63 binding sites proximal to
265 genes dependent on p63 expression suggests that p63 directly controls enhancer
266 activity (Supplemental Fig. S4B).
267 We then investigated additional mechanisms that might contribute to our
268 observations of p63-dependent enhancer activity. p63-bound enhancers with the
269 highest-dependence on p63 for H3K4me2 enrichment were significantly more likely to
270 overlap epithelial-specific DNase hypersensitive sites than those bound by p63, but not
271 affected by p63 depletion (Supplemental Fig. S4C, Supplemental Table S6). MCF10A-
272 specific p63 binding sites are strongly enriched for enhancer-associated modifications
273 across epithelial cell types (Supplemental Fig. S4D). The p63-insensitive enhancers
274 were broadly accessible across cell types, suggesting that these enhancers, while
275 bound by p63, are not p63 dependent (Fig. 4E). Indeed, analysis of transcription factor
276 motifs within p63-bound enhancers revealed a strong enrichment of ETS family
277 transcription factors in the p63-insensitive enhancers (Fig. 4F, Supplemental Table S7).
278 These data suggest that the activity of p63-insensitive enhancers is dependent on other
279 transcription factors. Therefore, our results demonstrate that p63 activity is critical for
280 local H3K27ac and H3K4me2 enrichment at a set of epithelial-specific enhancers and
281 that p63 binds to another set of cell type-independent enhancers putatively dependent
282 on transcription factor families like ETS. Combinatorial transcription factor binding at
283 enhancers is critical for appropriate spatial and temporal gene expression (Reiter et al.
284 2017; Shlyueva et al. 2014), and the collaborators at p53 family-bound enhancers are

285 relatively understudied compared to promoters(Sullivan et al. 2018). Recent *in vivo*
286 dissection of p53 enhancer activity implicated the general enhancer-associated AP-1
287 family member CEBPB as a direct regulator of an enhancer upstream of *CDKN1A*
288 (Korkmaz et al. 2016).
289 Our data indicates that p63 might be a pioneer factor for a set of epithelial-
290 specific enhancers, but not the entire complement of p63-bound enhancers. A number
291 of studies have demonstrated that p53 has partial pioneer factor activity as it can
292 directly bind its consensus sequence in the context of a nucleosome. p53 may possess
293 pioneering activity, but the large majority of p53 binding sites are constitutively closed or
294 are within accessible chromatin (Younger and Rinn 2017; Sammons et al. 2015;
295 Andrysik et al. 2017). Therefore, we examined whether p53 might serve pioneer or
296 maintenance roles at enhancers. Basal H3K4me2 and H3K27ac enrichment at p53
297 binding sites was essentially unaffected by the loss of p53 (Fig 4G). p63 knockdown led
298 to a loss of H3K27ac and H3K4me2 enrichment at p53 binding sites (Fig. 4G,
299 Supplemental Fig. S4E), an expected result as approximately 75% of p53 binding
300 events in MCF10A cells are also p63 binding sites (Fig. 3B). Examination of p53+/p63-
301 binding events displayed a similar outcome, with both H3K27ac and H3K4me2
302 unaffected by p53 loss (Supplemental Fig. S4F). Surprisingly, enhancer-associated
303 histone modifications at these sites were still partially dependent on p63 (Supplemental
304 Fig. S4F), potentially due to sub-peak threshold binding of p63. p53 is required for *de*
305 *novo* Nutlin-3A-induced H3K27ac levels at p53 binding sites (Fig. 4G-H). p63 depletion,
306 while affecting basal enrichment, has a milder effect on Nutlin-3A-induced H3K27ac
307 (Fig. 4G). p53 activation restores H3K27ac to near wild-type levels in p63-depleted
308 MCF10A (Fig. 4G). Consistent with p63 as both an activator and repressor of p53-
309 dependent transcription, basal levels of H3K27ac are reduced in the absence of p63 but
310 are derepressed upon p53 activation (Fig. 4G-H).
311 Epithelial cell types like MCF10A express multiple p53 family members that might
312 redundantly regulate enhancer activity. We therefore extended our analysis to isogenic
313 WT or *TP53*-/- HCT116 human colon carcinoma cell lines and WT or *Trp53*-/- mouse
314 embryonic fibroblasts (MEF). Both cell models lack endogenous p63 and thus should
315 allow us to define the role of p53 in enhancer maintenance and activity. Similar to our

316 observations in MCF10A cells, basal enhancer-associated H3K4me1/2 methylation at
317 p53-bound enhancers is unaffected by the loss of p53 (Fig. 4I-J). These data suggest
318 that p53 is not an enhancer maintenance factor and contributes primarily to *de novo*
319 histone acetylation and transcriptional activation at already established enhancers. p63,
320 on the other hand, is critical for maintenance of epithelial-specific enhancers and
321 positively influences p53 transcriptional activity through these *cis*-regulatory regions.
322 Therefore, p53 and p63 have both their previously reported antagonistic relationship
323 and a more broadly cooperative partnership than expected (Botchkarev and Flores
324 2014; Flores et al. 2002). The requirement of p63 for epithelial-specific p53 activity
325 supports a model whereby the p53-dependent transcriptome is licensed by the
326 enhancer regulatory abilities of other transcription factors. This model is a particularly
327 attractive avenue for further inquiry as it provides a straightforward mechanism for
328 driving cell type-dependent tumor suppressor and homeostatic activities of p53.
329
330

Materials and Methods

Cell Culture and Treatment

MCF10A mammalian epithelial cells and skin foreskin fibroblast cells (AG22153, Coriell Institute) were cultured at 37˚C in 5% CO_2 in HuMEC Complete media (Gibco, #12752010) and DMEM media (with 10% FBS and 1% Pen/Strep, Gibco), respectively. Wild-type and p53-knockout HCT116 colon carcinoma and mouse embryonic fibroblasts were kind gifts of Carol Prives and Jing Huang, respectively. To induce p53 activation, cells were treated with Nutlin-3A (5 μM final) or DMSO (vehicle control) for 6 hours.

Western Blotting

Cells were lysed in RIPA buffer (10 mM Tris-HCl (pH 8.0), 1 mM EDTA, 1% Triton X-100, 0.1% sodium deoxycholate, 0.1% SDS and 140 mM NaCl, supplemented freshly with protease inhibitors) and probed with antibodies against p53 (BD Biosciences; BD554293), p63 (Cell Signaling; 13102), and GAPDH (Cell Signaling; 5174).

Other detailed experimental procedures are described in the Supplemental Materials.

Data Availability

All raw data associated with this study are pending at NCBI Gene Expression Omnibus and accession numbers will be available upon publication.

Acknowledgments

We are grateful to Allison Catizone and Enrique Lin Shiao for critical feedback on this manuscript. We thank Jason Herschkowitz for the MCF10A cell line and the University at Albany CFG for sequencing support. This work is supported by start-up funds from the State University of New York at Albany.

355 **References**
356

357 Allen MA, Andrysik Z, Dengler VL, Mellert HS, Guarnieri A, Freeman JA, Sullivan KD,
358 Galbraith MD, Luo X, Kraus WL, et al. 2014. Global analysis of p53-regulated
359 transcription identifies its direct targets and unexpected regulatory mechanisms.
360 *Elife* **3**: e02200.

361 Andrysik Z, Galbraith MD, Guarnieri AL, Zaccara S, Sullivan KD, Pandey A, MacBeth M,
362 Inga A, Espinosa JM. 2017. Identification of a core TP53 transcriptional program
363 with highly distributed tumor suppressive activity. *Genome Res* **27**: 1645–1657.

364 Bao X, Rubin AJ, Qu K, Zhang J, Giresi PG, Chang HY, Khavari PA. 2015. A novel
365 ATAC-seq approach reveals lineage-specific reinforcement of the open
366 chromatin landscape via cooperation between BAF and p63. *Genome Biol* **16**:
367 284.

368 Billant O, Leon A, Le Guellec S, Friocourt G, Blondel M, Voisset C. 2016. The dominant-
369 negative interplay between p53, p63 and p73: A family affair. *Oncotarget* **7**:
370 69549–69564.

371 Botchkarev VA, Flores ER. 2014. p53/p63/p73 in the epidermis in health and disease.
372 *Cold Spring Harb Perspect Med* **4**.

373 Brunner HG, Hamel BC, Van Bokhoven H. 2002. The p63 gene in EEC and other
374 syndromes. *J Med Genet* **39**: 377–81.

375 Calo E, Wysocka J. 2013. Modification of Enhancer Chromatin: What, How, and Why?
376 *Mol Cell* **49**: 825–837.

377 Carroll DK, Carroll JS, Leong C-O, Cheng F, Brown M, Mills AA, Brugge JS, Ellisen LW.
378 2006. p63 regulates an adhesion programme and cell survival in epithelial cells.
379 *Nat Cell Biol* **8**: 551.

380 Ciriello G, Miller ML, Aksoy BA, Senbabaoglu Y, Schultz N, Sander C. 2013. Emerging
381 landscape of oncogenic signatures across human cancers. *Nat Genet* **45**: 1127–
382 33.

383 Cui F, Zhurkin VB. 2014. Rotational positioning of nucleosomes facilitates selective
384 binding of p53 to response elements associated with cell cycle arrest. *Nucleic*
385 *Acids Res* **42**: 836–47.

386 DeYoung MP, Ellisen LW. 2007. p63 and p73 in human cancer: defining the network.
387 *Oncogene* **26**: 5169–5183.

388 Fakhouri WD, Rahimov F, Attanasio C, Kouwenhoven EN, Ferreira De Lima RL, Felix
389 TM, Nitschke L, Huver D, Barrons J, Kousa YA, et al. 2014. An etiologic

390 regulatory mutation in IRF6 with loss- and gain-of-function effects. *Hum Mol*
391 *Genet* **23**: 2711–20.

392 Fischer M. 2017. Census and evaluation of p53 target genes. *Oncogene* **36**: 3943–
393 3956.

394 Flores ER, Tsai KY, Crowley D, Sengupta S, Yang A, McKeon F, Jacks T. 2002. p63
395 and p73 are required for p53-dependent apoptosis in response to DNA damage.
396 *Nature* **416**: 560–564.

397 Hafner A, Lahav G, Stewart-Ornstein J. 2017. Stereotyped p53 binding tuned by
398 chromatin accessibility. *bioRxiv* 177667.

399 Heinz S, Romanoski CE, Benner C, Glass CK. 2015. The selection and function of cell
400 type-specific enhancers. *Nat Rev Mol Cell Biol* **16**: 144–154.

401 Hermeking H, Lengauer C, Polyak K, He T-C, Zhang L, Thiagalingam S, Kinzler KW,
402 Vogelstein B. 1997. 14-3-3σ Is a p53-Regulated Inhibitor of G2/M Progression.
403 *Mol Cell* **1**: 3–11.

404 Kandoth C, McLellan MD, Vandin F, Ye K, Niu B, Lu C, Xie M, Zhang Q, McMichael JF,
405 Wyczalkowski MA, et al. 2013. Mutational landscape and significance across 12
406 major cancer types. *Nature* **502**: 333–9.

407 Kastenhuber ER, Lowe SW. 2017. Putting p53 in Context. *Cell* **170**: 1062–1078.

408 Kenzelmann Broz D, Spano Mello S, Bieging KT, Jiang D, Dusek RL, Brady CA, Sidow
409 A, Attardi LD. 2013. Global genomic profiling reveals an extensive p53-regulated
410 autophagy program contributing to key p53 responses. *Genes Dev* **27**: 1016–31.

411 Korkmaz G, Lopes R, Ugalde AP, Nevedomskaya E, Han R, Myacheva K, Zwart W,
412 Elkon R, Agami R. 2016. Functional genetic screens for enhancer elements in
413 the human genome using CRISPR-Cas9. *Nat Biotechnol* **34**: 192–198.

414 Kouwenhoven EN, Oti M, Niehues H, van Heeringen SJ, Schalkwijk J, Stunnenberg
415 HG, van Bokhoven H, Zhou H. 2015. Transcription factor p63 bookmarks and
416 regulates dynamic enhancers during epidermal differentiation. *EMBO Rep* **16**:
417 863–78.

418 Levrero M, Laurenzi VD, Costanzo A, Gong J, Wang JY, Melino G. 2000. The
419 p53/p63/p73 family of transcription factors: overlapping and distinct functions. *J*
420 *Cell Sci* **113**: 1661–1670.

421 Li T, Kon N, Jiang L, Tan M, Ludwig T, Zhao Y, Baer R, Gu W. 2012. Tumor
422 suppression in the absence of p53-mediated cell-cycle arrest, apoptosis, and
423 senescence. *Cell* **149**: 1269–83.

424 Lin-Shiao E, Lan Y, Coradin M, Anderson A, Donahue G, Simpson CL, Sen P, Saffie R,
425 Busino L, Garcia BA, et al. 2018. KMT2D regulates p63 target enhancers to
426 coordinate epithelial homeostasis. *Genes Dev* **32**: 181–193.

427 Melino G, Memmi EM, Pelicci PG, Bernassola F. 2015. Maintaining epithelial stemness
428 with p63. *Sci Signal* **8**: re9.

429 Moll UM, Erster S, Zaika A. 2001. p53, p63 and p73--solos, alliances and feuds among
430 family members. *Biochim Biophys Acta* **1552**: 47–59.

431 Mundt HM, Stremmel W, Melino G, Krammer PH, Schilling T, Müller M. 2010. Dominant
432 negative (DeltaN) p63alpha induces drug resistance in hepatocellular carcinoma
433 by interference with apoptosis signaling pathways. *Biochem Biophys Res*
434 *Commun* **396**: 335–341.

435 Mungamuri SK, Benson EK, Wang S, Gu W, Lee SW, Aaronson SA. 2012. p53-
436 mediated heterochromatin reorganization regulates its cell fate decisions. *Nat*
437 *Struct Mol Biol* **19**: 478–484.

438 París R, Henry RE, Stephens SJ, McBryde M, Espinosa JM. 2008. Multiple p53-
439 independent gene silencing mechanisms define the cellular response to p53
440 activation. *Cell Cycle* **7**: 2427–2433.

441 Reiter F, Wienerroither S, Stark A. 2017. Combinatorial function of transcription factors
442 and cofactors. *Curr Opin Genet Dev* **43**: 73–81.

443 Saladi SV, Ross K, Karaayvaz M, Tata PR, Mou H, Rajagopal J, Ramaswamy S, Ellisen
444 LW. 2017. ACTL6A Is Co-Amplified with p63 in Squamous Cell Carcinoma to
445 Drive YAP Activation, Regenerative Proliferation, and Poor Prognosis. *Cancer*
446 *Cell* **31**: 35–49.

447 Sammons MA, Zhu J, Drake AM, Berger SL. 2015. TP53 engagement with the genome
448 occurs in distinct local chromatin environments via pioneer factor activity.
449 *Genome Res* **25**: 179–88.

450 Shlyueva D, Stampfel G, Stark A. 2014. Transcriptional enhancers: from properties to
451 genome-wide predictions. *Nat Rev Genet* **15**: 272–286.

452 Sullivan KD, Galbraith MD, Andrysik Z, Espinosa JM. 2018. Mechanisms of
453 transcriptional regulation by p53. *Cell Death Differ* **25**: 133–143.

454 The FANTOM Consortium, Andersson R, Gebhard C, Miguel-Escalada I, Hoof I,
455 Bornholdt J, Boyd M, Chen Y, Zhao X, Schmidl C, et al. 2014. An atlas of active
456 enhancers across human cell types and tissues. *Nature* **507**: 455–461.

457 Vassilev LT, Vu BT, Graves B, Carvajal D, Podlaski F, Filipovic Z, Kong N, Kammlott U,
458 Lukacs C, Klein C, et al. 2004. In vivo activation of the p53 pathway by small-
459 molecule antagonists of MDM2. *Science* **303**: 844–848.

460 Verfaillie A, Svetlichnyy D, Imrichova H, Davie K, Fiers M, Kalender Atak Z, Hulselmans
461 G, Christiaens V, Aerts S. 2016. Multiplex enhancer-reporter assays uncover
462 unsophisticated TP53 enhancer logic. *Genome Res* **26**: 882–895.

463 Yang A, Kaghad M, Wang Y, Gillett E, Fleming MD, Dötsch V, Andrews NC, Caput D,
464 McKeon F. 1998. p63, a p53 Homolog at 3q27–29, Encodes Multiple Products
465 with Transactivating, Death-Inducing, and Dominant-Negative Activities. *Mol Cell*
466 **2**: 305–316.

467 Yang A, Schweitzer R, Sun D, Kaghad M, Walker N, Bronson RT, Tabin C, Sharpe A,
468 Caput D, Crum C, et al. 1999. p63 is essential for regenerative proliferation in
469 limb, craniofacial and epithelial development. *Nature* **398**: 714–8.

470 Yang A, Zhu Z, Kapranov P, McKeon F, Church GM, Gingeras TR, Struhl K. 2006.
471 Relationships between p63 Binding, DNA Sequence, Transcription Activity, and
472 Biological Function in Human Cells. *Mol Cell* **24**: 593–602.

473 Younger ST, Rinn JL. 2017. p53 regulates enhancer accessibility and activity in
474 response to DNA damage. *Nucleic Acids Res* **45**: 9889–9900.

475 Zhu J, Dou Z, Sammons MA, Levine AJ, Berger SL. 2016. Lysine methylation represses
476 p53 activity in teratocarcinoma cancer cells. *Proc Natl Acad Sci U S A* **113**:
477 9822–9827.

478

Figure 1

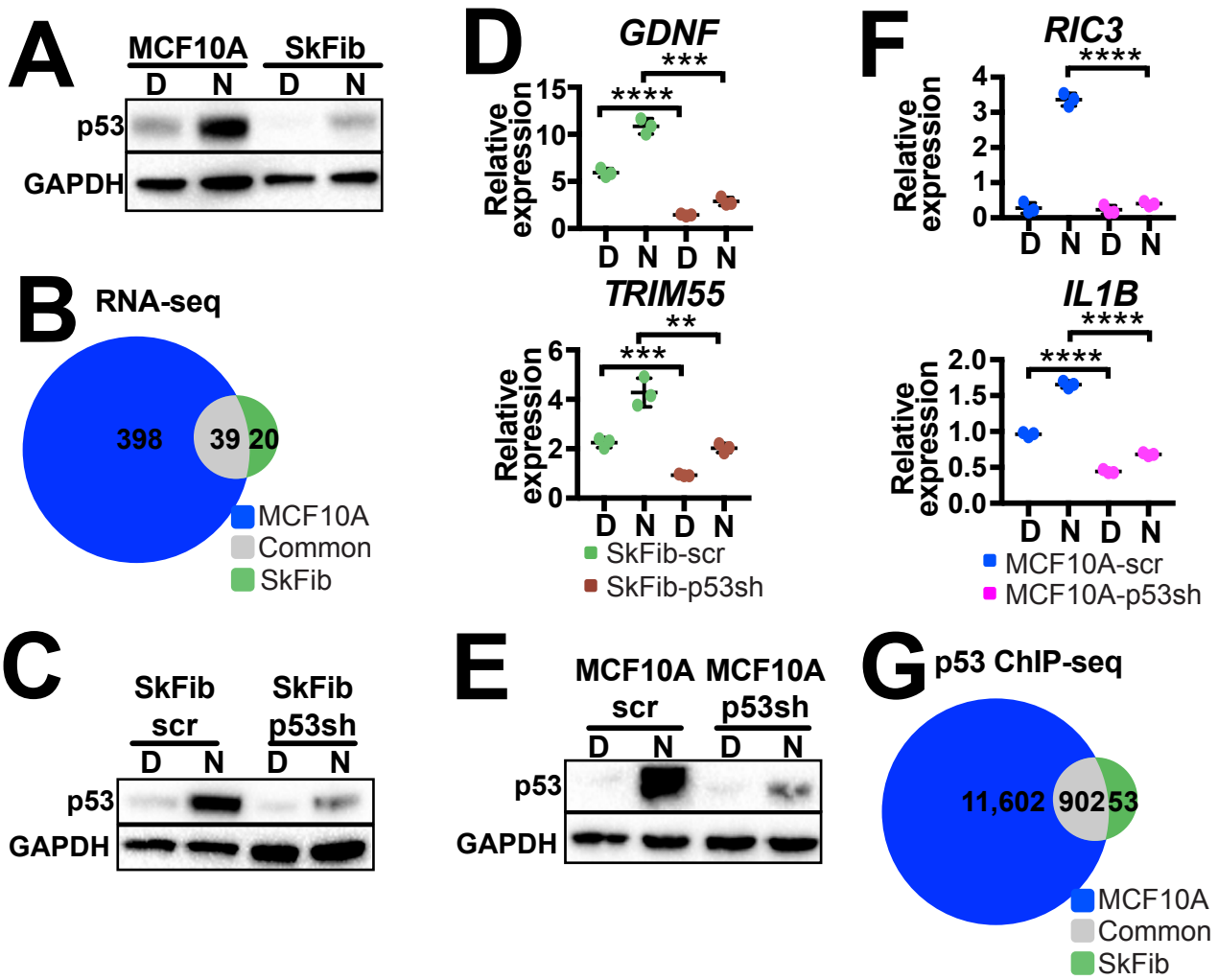

Figure 1. The p53 cistrome and transcriptome are cell type-dependent *(A)* Western blot of cell lysates from MCF10A or SkFib cells at 6 hours after DMSO or Nutlin-3A treatment. *(B)* Venn diagram indicating differentially upregulated genes (Nutlin-3a/DMSO, fold change >2, adjusted p<0.05) in MCF10A or SkFib cells. *(C)* Immunoblotting for p53 expression at 6 hours of DMSO (D) or Nutlin-3A (N) treatment in SkFib cells stably expressing shRNA against p53 (p53 sh) or a non-targeting control shRNA (scr). *(D)* qRT-PCR analysis of SkFib-specific gene targets, GDNF and TRIM55, in SkFib cells stably expressing an shRNA to p53 (p53 sh) or a non-targeting control shRNA (scr). Gene expression is normalized to GAPDH expression. Error bars represent SEM; ****p<0.0001, ***p<0.001 and **p<0.01, calculated by Student's t-test. *(E)* Immunoblotting for p53 expression at 6 hours of DMSO (D) or Nutlin-3A (N) treatment in response to p53 knockdown in MCF10A cells stably expressing shRNA against p53 or a non-targeting control shRNA (scr). *(F)* qRT-PCR analysis of MCF10A-specific Nutlin-3A-induced genes, RIC3 and IL1B, in MCF10A cells stably expressing an shRNA to p53 (p53 sh) or a non-targeting control shRNA (scr). Expression is normalized to GAPDH expression. Error bars represent SEM; ****p<0.0001, calculated by Student's t-test. *(G)* Venn diagram depicting overlap between significantly-enriched (p<0.01, MACS v2) Nutlin-3A-induced p53 peaks in MCF10A or SkFib.

Figure 2

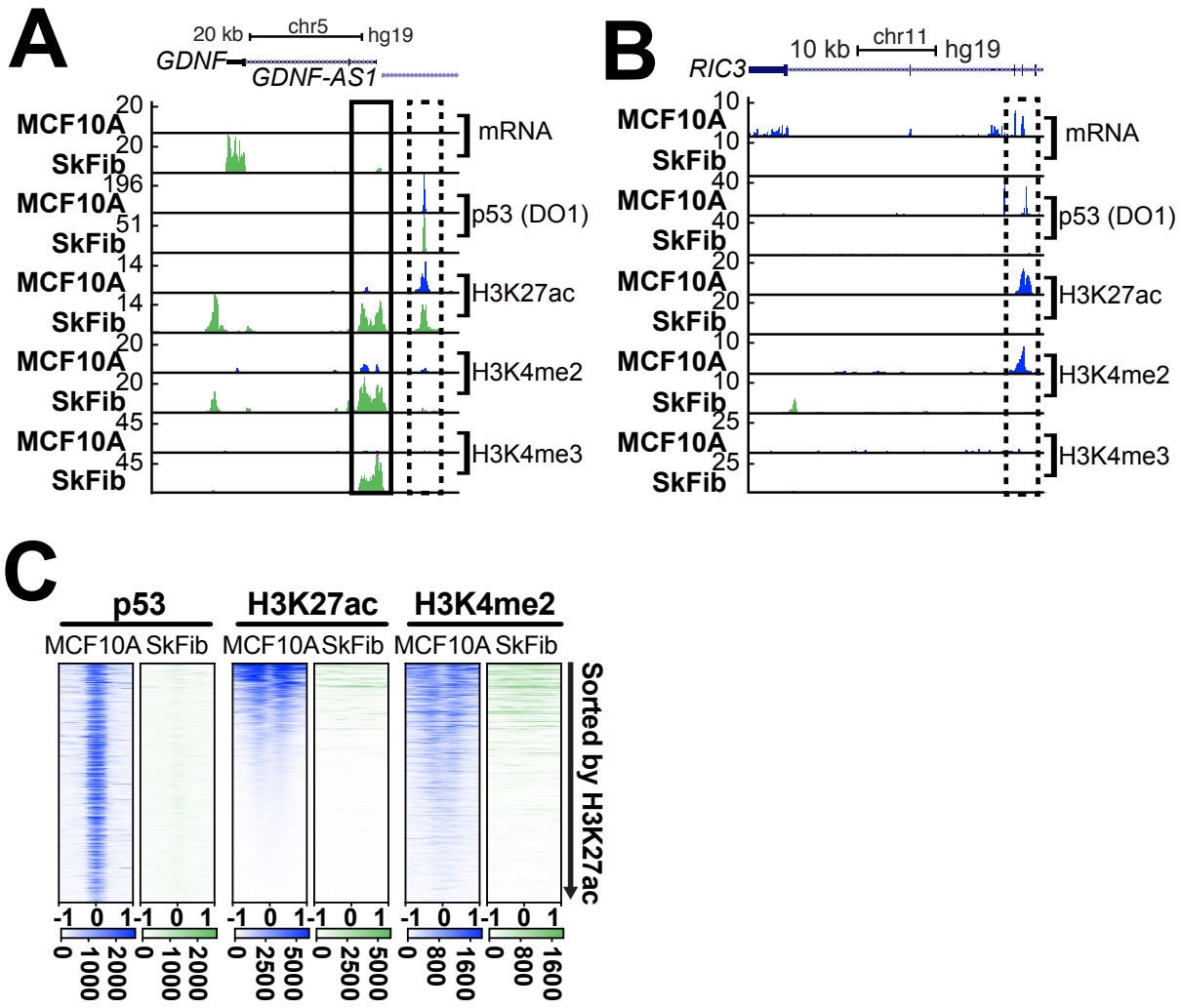

Figure 2. *Cis*-regulatory activity and differential p53 binding drives cell type-specific target gene expression. *(A)* Representative UCSC Genome Browser track view of the GDNF locus, a SkFib-specific p53 target. A p53-bound, putative enhancer (H3K27ac+, H3K4me2+, H3K4me3-) is bound by a dashed box, while the putative GDNF promoter (H3K27ac/H3K4me2/H3K4me3+) is bound by a solid box. The y-axis is scaled to the maximum intensity between MCF10A or SkFib for each feature. *(B)* Representative UCSC Genome Browser track view at the RIC3 locus, illustrating p53 binding to an MCF10A-specific enhancer signature (H3K27ac+, H3K4me2+, H3K4me3-) in response to Nutlin-3A treatment. The y-axis is scaled to the maximum intensity between MCF10A or SkFib for each feature. *(C)* Heatmap plots at MCF10A-specific p53 binding sites for p53, H3K27ac, and H3K4me2 enrichment in MCF10A or SkFib within a 2000-bp window (-/+ 1000 bp from the p53 motif; '-1' indicates 1000bp downstream from the motif, '0' indicates the motif center, and '+1' indicates 1000bp upstream from the motif).

Figure 3

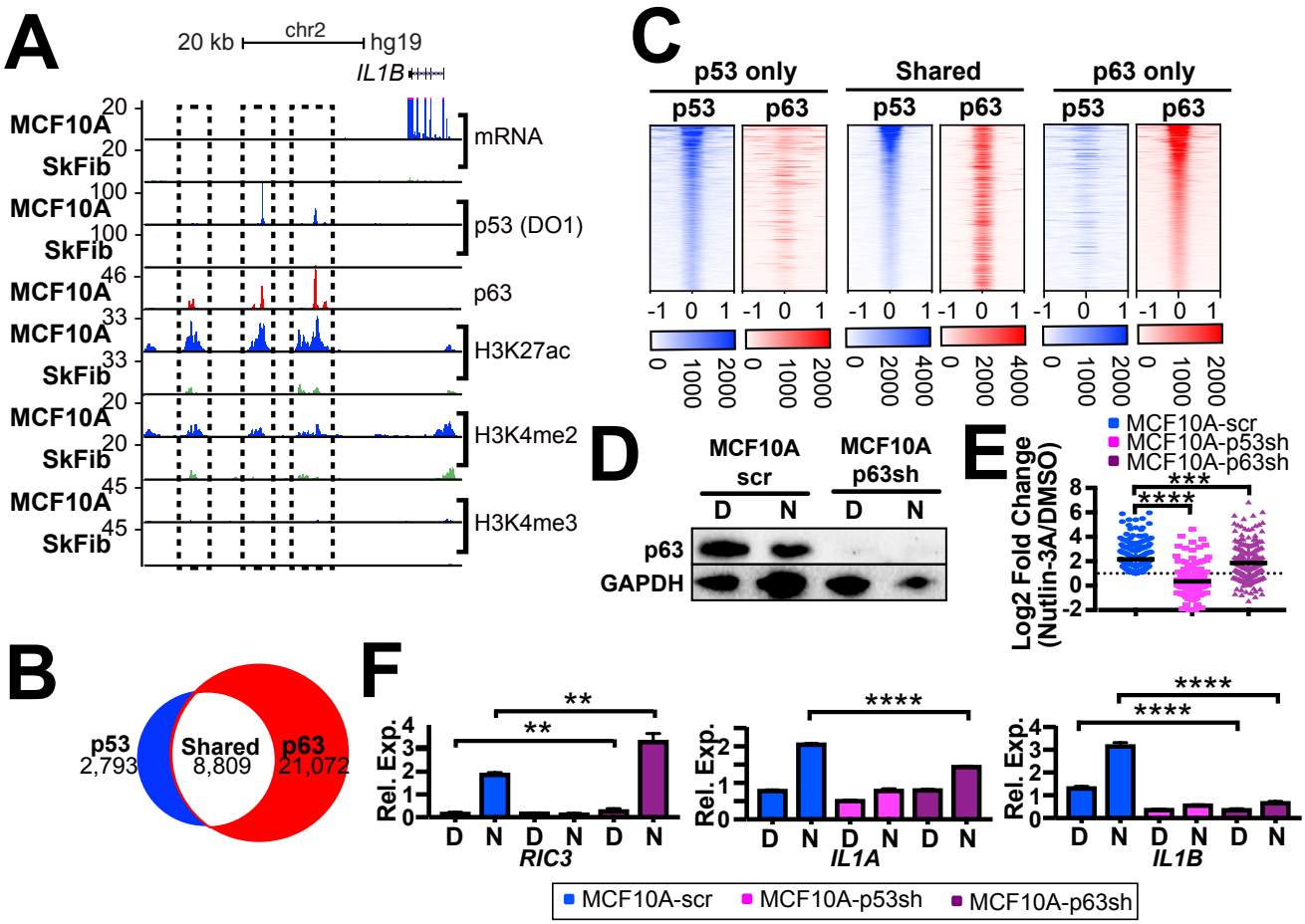

Figure 3. p63 engages with p53-bound enhancers and regulates p53-dependent trans-activation of epithelial target genes. *(A)* Representative UCSC Genome Browser track view of the IL1B locus, illustrating three MCF10A-specific putative enhancers bound by p53 and p63 in response to Nutlin-3A treatment (H3K27ac+, H3K4me2+, H3K4me3-; dashed box). The y-axis is scaled to the maximum intensity for each data set. *(B)* Venn diagram representation of the overlap between enriched p53 and p63 peaks (input-normalized, p53/p63 motif-positive, MACS v2, p<0.01) in MCF10A when treated with Nutlin-3A. *(C)* Heatmap plots of p53 and p63 enrichment at p53 only, shared, and p63 only binding sites in MCF10A cells within a 2000-bp window (-/+ 1000 bp from the p53 motif) in response to Nutlin-3A treatment. *(D)* Immunoblotting for p63 in response to p63 knockdown in MCF10A cells stably expressing shRNA to p63 or a non-targeting control shRNA (scr) after 6 hours of DMSO (D) or Nutlin-3A (N) treatment. *(E)* Fold-change (Nutlin-3A/DMSO, log2, median in black) of MCF10A-specific Nutlin-3A-induced genes in MCF10A cells expressing shRNA targeting either a non-targeting control (scr), p53, or p63. ****p<0.0001 and ***p<0.001 *(F)* qRT-PCR analysis of MCF10A-specific Nutlin-3A-induced genes, RIC3, IL1A and IL1B. Expression is normalized to GAPDH expression. Error bars represent SEM; ****p<0.0001 and **p<0.01, calculated by Student's t-test.

Figure 4

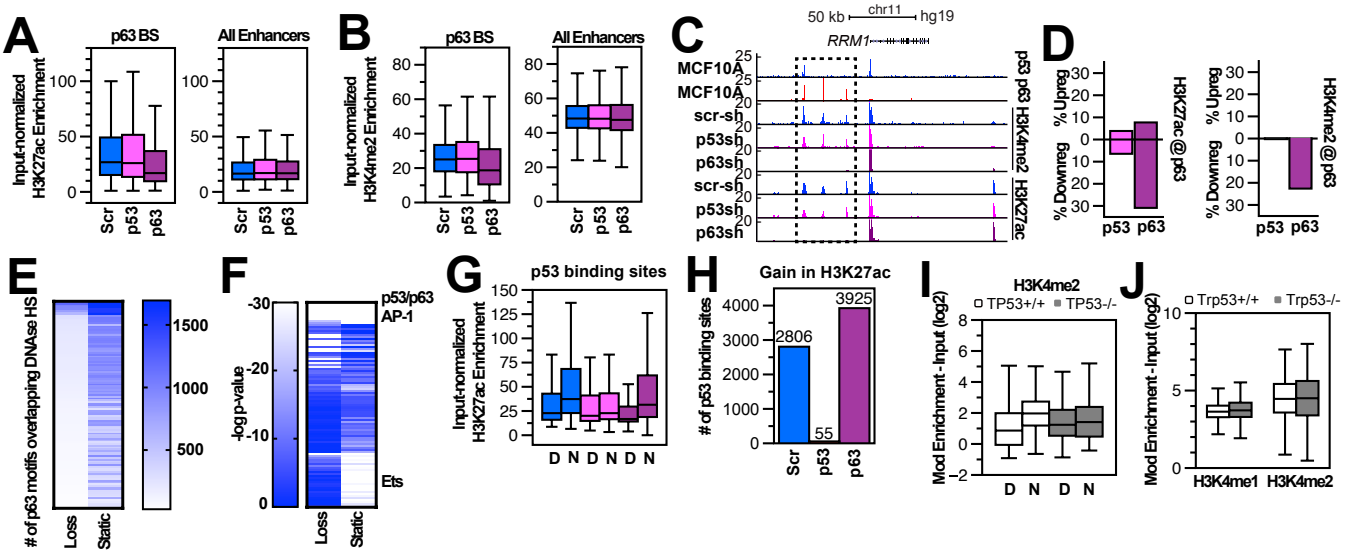

Figure 4: p63, and not p53, maintains enhancer chromatin identity. Input-subtracted *(A)* H327ac or *(B)* H3K4me2 enrichment at p63 binding sites (left, -/+ 250bp from p63 peak center) or at all remaining enhancers (H3K27ac+, H3K4me2+, H3K4me3-, right) in MCF10A cells expressing non-targeting (Scr), p53, or p63 shRNA. *(C)* Representative UCSC Genome Browser track view of the *RRM1* locus, illustrating three MCF10A-specific putative enhancers bound by p63 that are lost in response to p63 depletion (H3K27ac+, H3K4me2+, H3K4me3-; dashed box). The y-axis is scaled to the maximum intensity for each data set. *(D)* Bar graphs depicting the percent of p63 peaks that show 2-fold gains or losses of H3K27ac (left) or H3K4me2 (right) in response to either p53 or p63 depletion relative to non-targeting control shRNA. *(E)* Heatmap depicting the number of p63 binding sites that lose H3K4me2 (left) or remain constant (right) after p63 depletion that are found within regions of DNAse hypersensitivity (DHS) across multiple cell lines. *(F)* Heatmap illustrating the –log(10) p-value of motif enrichment found at p63 binding sites that lose H3K4me2 (left) or remain constant (right) after p63 depletion. *(G)* H3K27ac enrichment at p53 binding sites in MCF10A cells expressing the represented shRNA molecules. *(H)* Bar graph displaying the number of p53 binding sites with more than 2-fold change in H3K27ac enrichment after Nutlin-3A treatment of MCF10 cells expressing the indicated shRNA. *(I)* H3K4me2 enrichment at p53 binding sites (Verfaillie et al. 2016) in HCT116 *TP53+/+* or -/- cells in response to DMSO or Nutlin-3A treatment. *(J)* H3K4me1 and H3K4me2 enrichment at p53 binding sites (Kenzelmann Broz et al. 2013) in *Trp53+/+* or *Trp53-/-* mouse embryonic fibroblasts.

Supplemental Figure 1

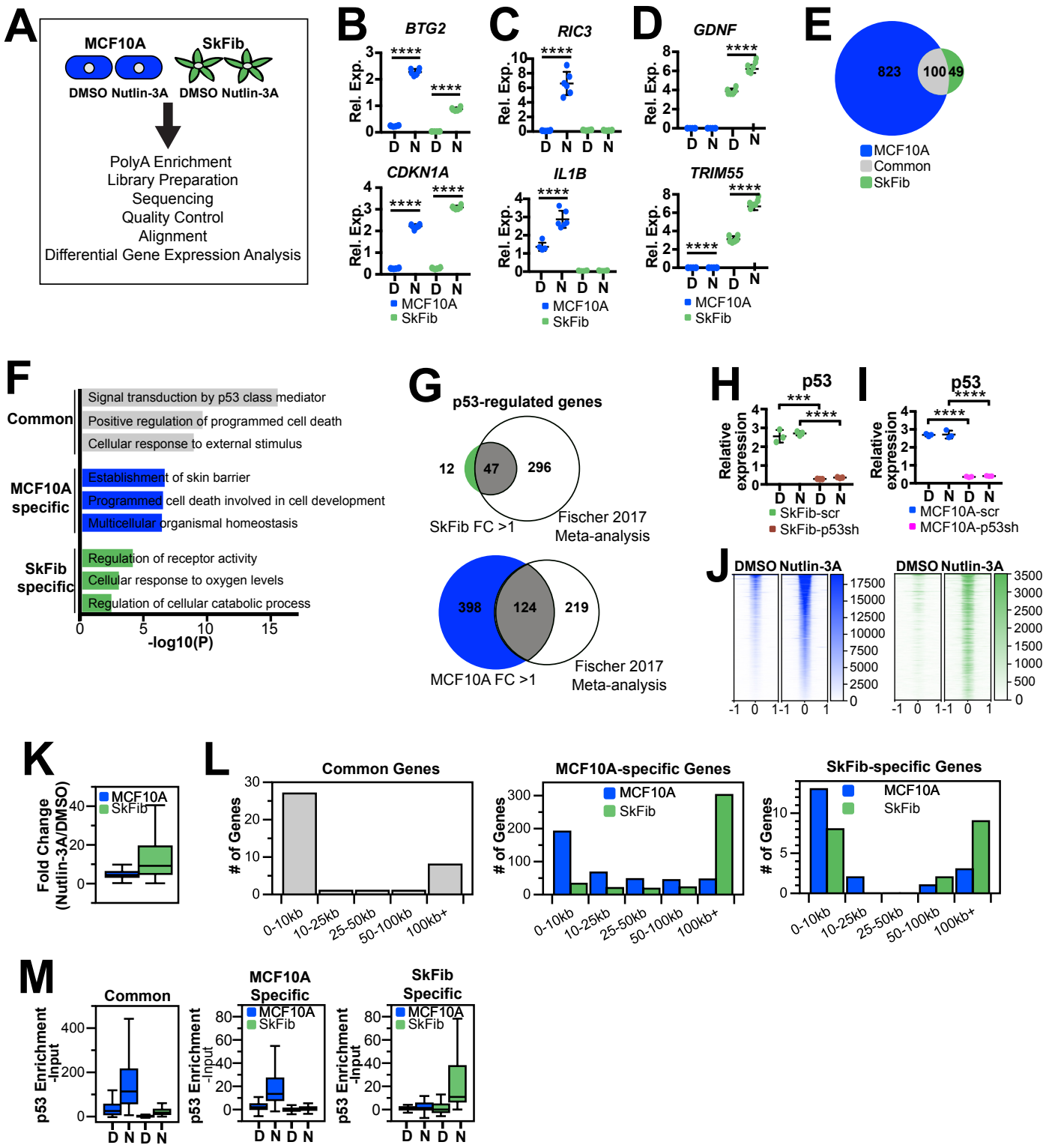

Supplemental Figure 2

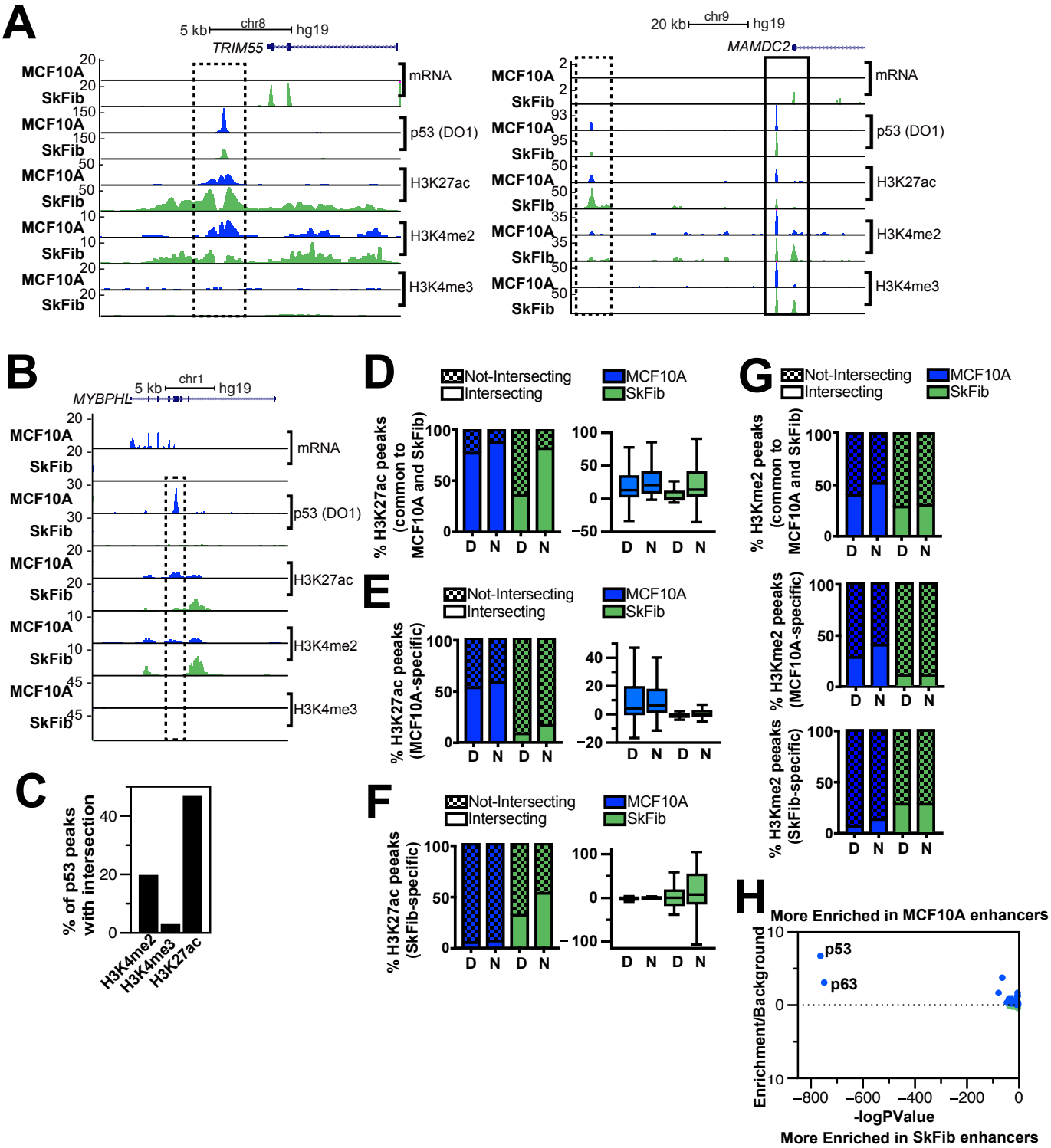

Supplemental Figure 3

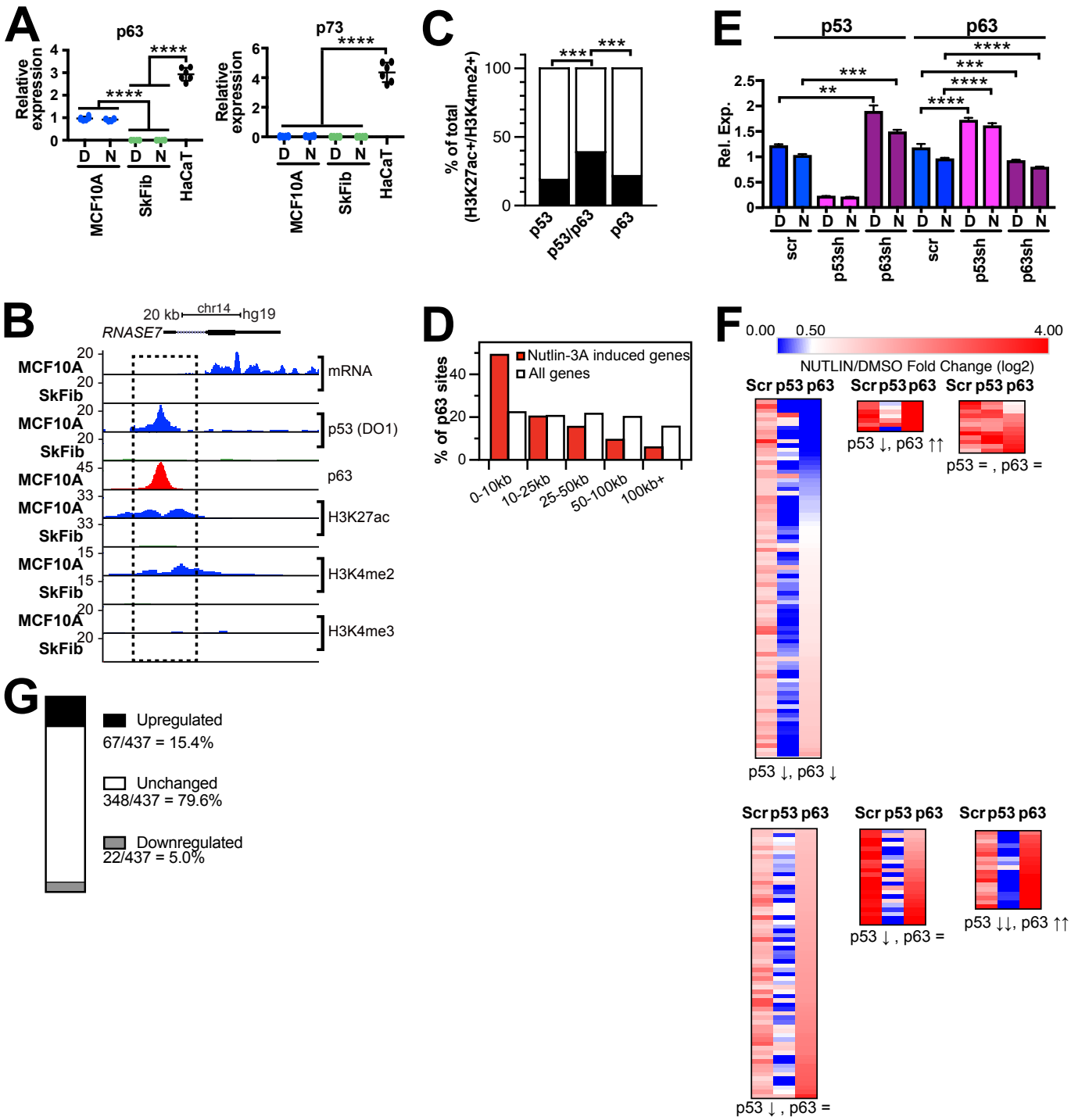

Supplemental Figure 4

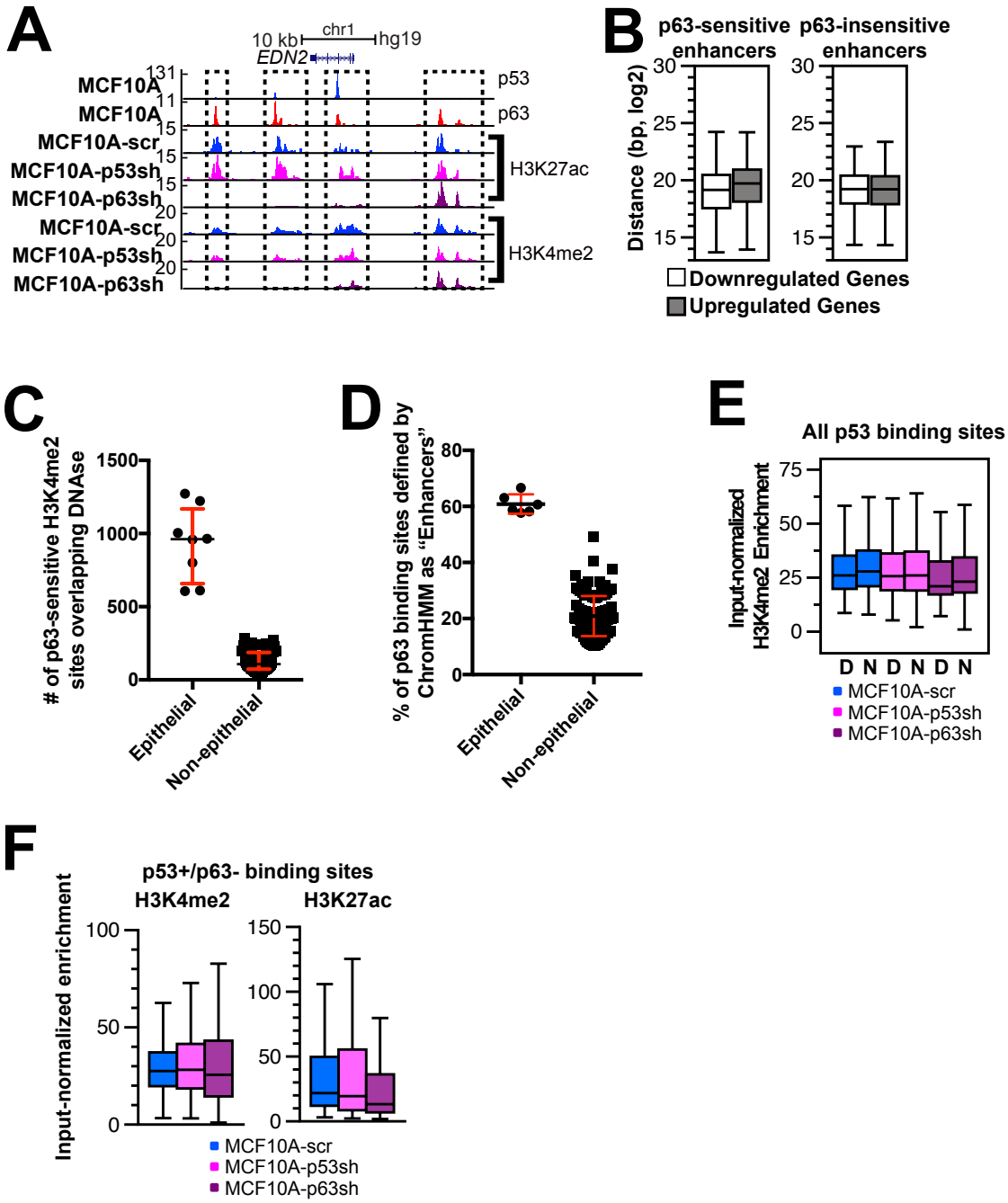

Supplemental Figure S1. Cell type-dependent p53 transcription in MCF10A and SkFib. *(A)* Experimental design for RNA-sequencing analysis in response to p53 activation by DMSO or 5μM Nutlin-3A for 6 hours. (B-D) qRT-PCR validation of two representative *(B)* common, *(C)* MCF10A, and *(D)* SkFib-specific Nutlin-3A-induced targets. Target gene expression is normalized to GAPDH and data represent technical replicates from three independent biological replicates. Error bars represent SEM with p values calculated by Student's t-test, ****p<0.0001. *(E)* Venn diagram indicating differentially upregulated genes (Nutlin-3a/DMSO, fold change >2, adjusted p<0.05) in MCF10A or SkFib cells. *(F)* Gene ontology analysis of differentially expressed genes from MCF10A and SkFib cells showing upregulated genes for top three significant biological processes. *(G)* Intersection between SkFib (top) or MCF10A (bottom) p53 targets identified in this work compared to the meta-analysis of p53 targets identified in at least 3 independent experiments (Fischer, M 2017). *(H)* qRT-PCR analysis of p53 expression at 6 hours of DMSO (D) or Nutlin-3A (N) treatment in SkFib cells stably expressing shRNA against p53 (p53 sh) or a non-targeting control shRNA (scr). p53 expression is normalized to GAPDH expression (Relative expression). Error bars represent SEM; ****p<0.0001 and ***p<0.001, calculated by Student's t-test. *(I)* qRT-PCR analysis of p53 expression at 6 hours of DMSO (D) or Nutlin-3A (N) treatment in response to p53 knockdown in MCF10A cells stably expressing shRNA against p53 or a non-targeting control shRNA (scr). p53 RNA expression is normalized to GAPDH expression. Error bars represent SEM; ****p<0.0001, calculated by Student's t-test. *(J)* Heatmap of input-subtracted p53 enrichment for MCF10A (blue, left) or SkFib (green, right) within a 2000-bp window (-/+ 1000 bp from the p53 motif; '-1' indicates 1000bp downstream from the motif, '0' indicates the motif center, and '+1' indicates 1000bp upstream from the motif). *(K)* Fold change ratio of Nutlin-3A/DMSO of common input-subtracted p53 enrichment for MCF10A or SkFib. *(L)* The percentage of p53 peaks common in MCF10A and SkFib (left), or only in MCF10A (middle), or only in SkFib (right) in response to Nutlin-3A treatment within varying distances to the nearest transcription start site (TSS) of a Nutlin-3A-induced gene. *(M)* Boxplot analysis of the input-subtracted p53 enrichment for MCF10A (blue) or SkFib (green) cells for common-(left), or MCF10A-specific-(middle), or SkFib-specific-p53 binding sites (right) in response to DMSO (D) or Nutlin-3A (N) treatment.

Supplemental Figure S2. Epigenomic analysis of cell type-dependent p53 activation. *(A)* Representative UCSC Genome Browser track view of TRIM55 and MAMDC2 loci, two fibroblast-specific p53 targets. p53-bound, putative enhancers (H3K27ac+, H3K4me2+, H3K4me3-) illustrated by dashed box for TRIM55 and MAMDC2, while the putative MAMDC2 promoter (H3K27ac/H3K4me2/H3K4me3+) is bound by a solid box. The y-axis is scaled to the maximum intensity between MCF10A or SkFib for each feature. *(B)* Representative UCSC Genome Browser track view at the MYBPHL locus, demonstrating an MCF10A-specific enhancer signature (H3K27ac+,H3K4me2+, H3K4me3-) at a p53 peak in response to Nutlin-3A treatment. The y-axis is scaled to the maximum intensity between MCF10A or SkFib for each feature. *(C)* The percentage of MCF10A p53 binding sites overlapping H3K4me2, H3K4me3, or H3K27ac under basal (DMSO-treated) conditions. (D-F) The percentage of intersecting H3K27ac peaks (input-normalized, MACS v2, p<0.01) with p53 peaks (input-normalized, MACS v2, p<0.01) that are *(D)* common to MCF10A and SkFib, *(E)* MCF10A-specific, or *(F)* SkFib-specific in response to DMSO (D) or Nutlin-3A (N) treatment. Adjacent boxplots depict H3K27ac enrichment over a 500bp window from the p53-binding site. *(G)* The percentage of intersecting H3K4me3 peaks (input-normalized, MACS v2, p<0.01) with p53 peaks (input-normalized, MACS v2, p<0.01) that are common to MCF10A and SkFib (top), MCF10A-specific (middle), or SkFib-specific (bottom) in response to DMSO (D) or Nutlin-3A (N) treatment. *(H)* Homer-derived transcription factor motif enrichment found in MCF10A (top) or SkFib (bottom) specific enhancers

Supplemental Figure S3. Epithelial-specific p53 binding sites correlate with p63 binding. *(A)* qRT-PCR analysis of p53, p63 or p73 of cell lysates from MCF10A, SkFib, HUVEC and HaCaT cells at 6 hours after DMSO (D) or Nutlin-3A (N) treatment. Expressions detected by qRT-PCR are normalized to GAPDH expression. HaCaT cells used as positive control for p63 and p73 expression. Error bars represent SEM, p values were calculated by Student's t-test, ****p<0.0001. *(B)* Representative UCSC Genome Browser track view of the RNASE7 locus, illustrating a MCF10A-specific putative enhancer bound by p53 and p63 in response to Nutlin-3A treatment (H3K27Ac+, H3K4me2+, H3K4me3-; dashed box). The y-axis is scaled to the maximum intensity for each data set. *(C)* The percentage of intersecting H3K27ac peaks (input-normalized, MACS v2, p<0.01) with p63 peaks observed in MCF10A cells (input-normalized, MACS v2, p<0.01) in response to DMSO (D) or Nutlin-3A (N) treatment. *(D)* The percentage of p63 binding sites observed in MCF10A cells at varying distances to the nearest TSS of all RefSeq genes (white) or Nutlin-3A induced genes (red). *(E)* qRT-PCR (right) analysis of p53 and p63 in response to p63 knockdown in MCF10A cells stably expressing shRNA to p63 or a non-targeting control shRNA (scr) after 6 hours of DMSO (D) or Nutlin-3A (N) treatment. Target gene expression is normalized to GAPDH for qRT-PCR analysis. Error bars represent SEM, p values were calculated by Student's t-test, ****p<0.0001, ***p<0.001 and **p<0.01. *(F)* K-means clustering of Nutlin-3A/DMSO fold-change values of previously identified MCF10A-specific p53 targets in MCF10A cells expressing either control (scr), p53, or p63-targeted shRNA. *(G)* The number and percent of p53 target genes showing downregulated, upregulated, or unchanged basal mRNA expression in MCF10A-p63KD cell lines.

Supplemental Figure S4. p63 is an enhancer maintenance factor.
(A) Representative UCSC Genome Browser track view of the EDN2 locus, illustrating three MCF10A-specific putative enhancers bound by p63 that are lost in response to p63 depletion (H3K27ac+, H3K4me2+, H3K4me3-; three separate dashed box). The y-axis is scaled to the maximum intensity for each data set. *(B)* The number of p63-sensitive, H3K4me2-marked enhancers (out of 1496 total) overlapping DNAse hypersensitive sites (DHS) across epithelial and non-epithelial cell types analyzed by the ENCODE project. Error bars represent the median and 95% confidence interval. *(C)* The percentage of all MCF10A p63 binding sites intersecting ChromHMM-derived “Enhancer” chromatin states in epithelial and non-epithelial cell types. *(D)* The distance (base pairs, log2) between p63-sensitive (left) or p63-insensitive (right) H3K4me2-marked enhancers and genes upregulated or downregulated in response to p63 depletion in MCF10A cells. *(E)* H3K4me2 enrichment (Input-subtracted H3K4me2, -/+ 250bp from p53 motif center) at p53 binding sites in MCF10A cells expressing control (scr), p53, or p63-targeted shRNA in response to DMSO or Nutlin-3A treatment. *(F)* Enrichment of H3K4me2 (left) or H3K27ac (right) at MCF10A p53+/p63- binding sites in in MCF10A cells expressing control (scr), p53, or p63-targeted shRNA in response to DMSO treatment. H3K4me2 and H3K27ac enrichment are reported as input-subtracted histone modification within a -/+ 250bp window from the p53 motif center.

Supplemental Materials for Karsli Uzunbas et al.

Methods

RNA-sequencing sample and library preparation

Total mRNA was extracted with E.Z.N.A. Total RNA kit (Omega; R6834-02) and Poly(A)+ RNA was isolated by double selection with poly-dT beads, using 2.5 μg total RNA, which is then followed by first- and second-strand synthesis. Sequencing libraries were prepared using NEXTflex Rapid Illumina DNA-Seq Library Prep Kit (Bioo Scientific). Samples were single-end sequenced on an NextSeq 500. RNA-seq reads were aligned via STAR (Dobin et al. 2013) to Ensembl v.75/hg19. Count tables were generated using STAR-aligned BAM files and HTseq (Anders et al. 2015). Count tables were then used to call differentially expressed genes using DEseq2 (Love et al. 2014).

Quantitative Real-Time PCR

Total RNA was extracted as per RNA-sequencing protocol and cDNA was synthesized using 1ug of total RNA as a template and the High-Capacity cDNA Reverse Transcription Kit (Applied Biosystems; 413760). Relative standard qPCR was performed using iTaq Universal SYBR Green Supermix (Bio-Rad; 172-5124) with primers shown in Supplemental Table S8 on an ABI 7900HT instrument.

Lentivirus production, purification and transduction

Lentiviral shRNAs were produced using HEK293T cells that were seeded in 6 well plates. shRNA sequences are as follows: p53 (GTCCAGATGAAGCTCCCAGAA), p63 (CCGTTTCGTCAGAACACACAT). 1 μg of pLKO plasmid having either scramble shRNA or p53 shRNA or p63 shRNA was combined with 1 μg mix of packaging plasmids (pMD2 and psPAX2) and the mixture was diluted into jetPRIME buffer (Polyplus Transfection; 89129-924) and reagents, following the manufacturer's protocol. Lentivirus containing supernatants were collected at 24 hours and 48 hours post-transfection, and filtered through a 0.45 μm membrane and stored in aliquots at -80°C. MCF10A or SkFib cells were transfected with lentivirus supplemented with 8 μg/ml

polybrene. At 24 hour post-infection with lentivirus, media was replaced with the proper puromycin selection (0.5 μg/ml for MCF10A and 2 μg/ml for SkFib).

ChIP-sequencing sample and library preparation

Cells were crosslinked at 80% confluency with 1% formaldehyde for 10 min at room temperature. Crosslinking was quenched with 125mM glycine and the resulting pellet was washed twice with cold PBS and lysed as previously described (Lee et al. 2006). Samples were subjected to sonication with Diagenode Bioruptor Plus for 40 cycles (30 sec on/off at high setting) for shearing chromatin to 150-500 bp average size.

Immunoprecipitation reactions for SkFib, MCF10A, and HCT116 cell lines were performed with Diagenode IP-Star Compact Automated System, with the exception of p53 ChIP experiments. Mouse embryonic fibroblast and p53 ChIP-seq were performed as described in Sammons et al 2015 (Sammons et al. 2015). Antibodies were preconjugated to Protein G beads (Invitrogen) against p63 (Cell Signaling; 13102), H3K4me1 (Abcam, ab8895), H3K4me3 (Active Motif; 39159), H3K4me2 (Millipore; 07-030), H3K27ac (Active Motif, 39133), p53 monoclonal antibody DO1 (BD Biosciences; BD554293). Immunoprecipitated DNA was reverse-crosslinked at 65°C for 4 hours, eluted, purified using SPRI beads, and used to construct sequencing libraries.

Sequencing libraries were prepared using NEBNext Ultra DNA Library Prep Kit for Illumina (New England Biolabs). Prior to sequencing, library quality control was performed with Qubit (Thermo Fisher Scientific), Bioanalyzer (Agilent) and qPCR quantification. All ChIP samples, including input, were single-end sequenced on an NextSeq 500 at the University at Albany Center for Functional Genomics. Uniquely aligned reads (up to one mismatch) were aligned to NCBI37/hg19 using Bowtie2 (Langmead and Salzberg 2012).

ChIP-seq Peak Calling

Significant regions of transcription factor (p53, p63) and histone modification (H3K4me2, H3K4me3, H3K27ac) enrichment were called using macs v.2.1.0 (Zhang et al. 2008) preserving only peaks with an adjusted P-value < 0.01. All peak calling was performed with sheared chromatin input. p53 and p63 motif analysis was performed using p53scan (Smeenk et al. 2008) and all macs-derived peaks lacking a p53/p63

consensus motif were removed from further analysis. A full list of p53/p63 peaks can be found in Supplemental Table S9. Global transcription factor motif enrichment experiments were performed using the findMotifsGenome.pl script from HOMER (Heinz et al. 2010).

Analysis of chromatin enrichment

Chromatin enrichment analyses were performed using the annotatePeaks.pl script of HOMER. Read-depth-scaled chromatin tag enrichment within a specified window was input-normalized (target – input) and then further scaled to total genomewide enrichment of peaks for that histone modification.

Computational Analysis and Plotting

Peak file intersections were performed using the intersectBed package of BedTools (Quinlan and Hall 2010), scoring positive intersections as those with at least 1bp of overlap (-f 1E-9). The original peak file (-a) was reported only once (-u) if any intersection exists with the query file (-b). The closestBed package of BedTools was used to measure distances between features with the distance reported using the –d option. Figures were generated using Graphpad Prism or Datagraph. Bigwig (bw) files were generated with the bamCoverage package of deepTools v.2.5.4 (Ramírez et al. 2016) with a bin size of 1 (--binSize 1) and read extension (--extendReads 300). Heatmaps were then generated using bigwig files for a -/+ 1000bp region from the p53/p63 peak center using the computeMatrix (reference-point, -a 1000, -b 1000, --binSize 10) and plotHeatmap functions. Genome browser tracks (bedGraph) were generated using the makeUCSCfile.pl package of HOMER (Heinz et al. 2010). K-means clustering was performed using cluster 3.0 for Mac.

Statistical Testing

Statistical testing was performed using Graphpad Prism (v. 7) or using built-in statistical parameters in *R* (v.3.4.0).

ChromHMM chromatin state and DNAse hypersensitive site (DHS) enrichment analysis

ChromHMM analysis (Ernst and Kellis 2012) was performed using the 25 state model (http://egg2.wustl.edu/roadmap/web_portal/), with at least 50% of the p53/p63 motif required to overlap a single chromatin enrichment term (closestBed –a p53.file –b ChromHMM.file –d –f 0.51). The 25 chromatin state models for ChromHMM terms were combined into 4 regulatory terms: enhancer, repressive, quiescent, or transcription. A full list of p53, p63, and p53/p63 binding site regulatory region inferences across the 127 cell types of the ChromHMM analysis can be found in Supplemental Table 10. DHS data were downloaded from http://hgdownload.cse.ucsc.edu/goldenpath/hg19/encodeDCC/wgEncodeRegDnaseClustered/. Intersection of p53/p63 peaks with DHS data was performed using the closetBed package of BedTools, with 100% of the p53/p63 motif required to overlap the DHS (-f 1).

Supplemental References

Anders S, Pyl PT, Huber W. 2015. HTSeq--a Python framework to work with high-throughput sequencing data. *Bioinforma Oxf Engl* **31**: 166–169.

Dobin A, Davis CA, Schlesinger F, Drenkow J, Zaleski C, Jha S, Batut P, Chaisson M, Gingeras TR. 2013. STAR: ultrafast universal RNA-seq aligner. *Bioinforma Oxf Engl* **29**: 15–21.

Ernst J, Kellis M. 2012. ChromHMM: automating chromatin-state discovery and characterization. *Nat Methods* **9**: 215–216.

Heinz S, Benner C, Spann N, Bertolino E, Lin YC, Laslo P, Cheng JX, Murre C, Singh H, Glass CK. 2010. Simple combinations of lineage-determining transcription factors prime cis-regulatory elements required for macrophage and B cell identities. *Mol Cell* **38**: 576–589.

Langmead B, Salzberg SL. 2012. Fast gapped-read alignment with Bowtie 2. *Nat Methods* **9**: 357–359.

Lee TI, Johnstone SE, Young RA. 2006. Chromatin immunoprecipitation and microarray-based analysis of protein location. *Nat Protoc* **1**: 729–748.

Love MI, Huber W, Anders S. 2014. Moderated estimation of fold change and dispersion for RNA-seq data with DESeq2. *Genome Biol* **15**: 550.

Quinlan AR, Hall IM. 2010. BEDTools: a flexible suite of utilities for comparing genomic features. *Bioinformatics* **26**: 841–842.

Ramírez F, Ryan DP, Grüning B, Bhardwaj V, Kilpert F, Richter AS, Heyne S, Dündar F, Manke T. 2016. deepTools2: a next generation web server for deep-sequencing data analysis. *Nucleic Acids Res* **44**: W160–W165.

Sammons MA, Zhu J, Drake AM, Berger SL. 2015. TP53 engagement with the genome occurs in distinct local chromatin environments via pioneer factor activity. *Genome Res* **25**: 179–188.

Smeenk L, van Heeringen SJ, Koeppel M, van Driel MA, Bartels SJ, Akkers RC, Denissov S, Stunnenberg HG, Lohrum M. 2008. Characterization of genome-wide p53-binding sites upon stress response. *Nucleic Acids Res* **36**: 3639–54.

Zhang Y, Liu T, Meyer CA, Eeckhoute J, Johnson DS, Bernstein BE, Nusbaum C, Myers RM, Brown M, Li W, et al. 2008. Model-based analysis of ChIP-Seq (MACS). *Genome Biol* **9**: R137.